Journal of Applied Polymer Science

Polyimide-based porous hollow carbon nanofibers for supercapacitor electrode

Trung Hieu Le,[1] Ying Yang,[1] Liu Yu,[1] Tianji Gao,[1] Zhenghong Huang,[2] Feiyu Kang[2]

[1]State Key Laboratory of Control and Simulation of Power System and Generation Equipments, Tsinghua University, Beijing 100084, China

[2]Laboratory of Advanced Materials Department of Materials Science and Engineering, Tsinghua University, Beijing 100084, China

Correspondence to: Y. Yang (E-mail: yingyang@tsinghua.edu.cn)

ABSTRACT: Porous hollow carbon nanofibers (PHCNFs) using styrene-acrylonitrile copolymer (SAN) solution as core and polyacrylic acid (PAA) as shell were manufactured by co-axial electrospinning technique, taking polyvinyl pyrrolidone (PVP) as a pore inducer additive in the shell. The shell thickness of PHCNFs could be adjusted by controlling flow rates of core and shell fluids. The prepared PHCNFs showed excellent electrochemical properties with the high specific capacitance of 221 F g^{-1} and superior cycling stability, remaining a capacitance retention of 95% after 5000 cycles under a scan rate of 0.1 V s^{-1}. In this system, hollow structures bring a 20% capacitance improvement, while the porous morphology brings a 47% capacitance improvement. The attractive performances exhibited by these sponge supercapacitors make them potentially promising candidates for future energy storage systems. © 2016 Wiley Periodicals, Inc. J. Appl. Polym. Sci. **2016**, *133*, 43397.

KEYWORDS: blends; electrospinning; fibers; membranes; polyimides

Received 18 September 2015; accepted 2 January 2016
DOI: 10.1002/app.43397

INTRODUCTION

Supercapacitors are important high power electrochemical energy storage devices.[1] Carbon materials have been investigated as one of the most promising electrodes candidates. Energy storage in carbon electrode is based on the electrostatic adsorption of electrolyte ions on the large specific surface area of electrically conductive porous electrodes.[2] Many efforts have been made to develop reasonable pore structure and pore distribution to improve the electrochemical behavior of carbon materials. The mechanism of electrolyte ion transportation within porous materials is related to the inner-pore ion transport resistance and diffusion distance.[3] A common method for reducing the ions transportation distance in micropores is to develop mesopores or macropores, which serve as ion-buffering reservoirs and provide convenient ion-transportation pathways into the micropores. Such an interconnected micro-, meso-, and macroporous network exhibits the advantages of each pore size during the charge–discharge process.[4,5]

Various hierarchically structured carbon, such as carbon nanotube arrays, hollow microspheres, and needle-like nanowires, have been successfully obtained with excellent electrochemical performance. Lai *et al.* reported that carbon hollow spheres with micropore shells and meso/macropore cores exhibit a specific capacitance of 270 F g^{-1} at a current density of 0.5 A g^{-1} in KOH aqueous electrolyte with a long cyclic life.[6] Han *et al.* prepared porous nitrogen-doped hollow carbon spheres with a specific surface area of 213 m^2 g^{-1} and a pore volume of 0.24 cm^3 g^{-1}. They found that the specific capacitance of the electrode prepared with such kind of porous hollow spheres was 213 F g^{-1} in 6*M* KOH aqueous electrolyte at a current density of 0.5 A g^{-1}. The capacity retention after 5000 charge/discharge cycles at a current density of 1 A g^{-1} is more than 91%.[7] Nevertheless, the development of facile and effective methods to obtain carbon materials with hollow nanostructures is still a great challenge.

As reported, polymer blend technique was proposed as one of the controllable and cost-effective methods for designing porous carbon materials.[8] Electrospinning is a promising and straightforward technique that produces continuous fibers with diameters in the range of nanometers to a few micrometers. Electrospun fibers possess large surface area-to-volume ratios.[9] To develop porous carbon nanofibers, polyvinyl pyrrolidone (PVP),[10–12] poly(methyl methacrylate) (PMMA),[13,14] and styrene-acrylonitrile copolymer (SAN)[15] have already been reported as pore inducer in electrospinning solution. Hollow carbon fibers could be produced by electrospinning technology with a two different electrospinnable materials and further carbonization to remove the inner material after co-axial electrospinning[11,15–17] for different applications. However, the approach to produce porous hollow

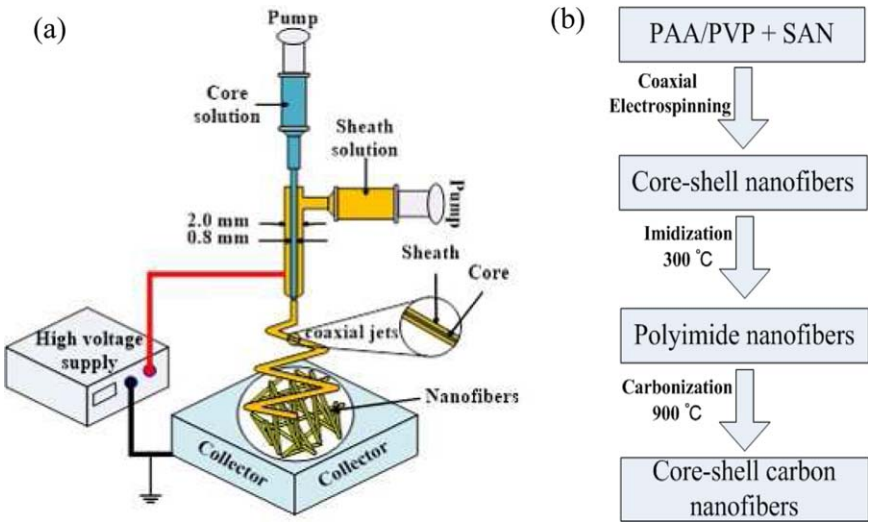

Figure 1. (a) schematic diagram of co-axial electrospinning device; (b) procedures of fabrication. [Color figure can be viewed in the online issue, which is available at wileyonlinelibrary.com.]

fibers and the properties of hollow carbon nanofibers are still unknown until now.

In this article, we prepared a polyimide (PI)-based self-supported and binder-free non-woven carbon fibers with a hollow and porous structure by co-axial electrospinning technology and further carbonization process. The most crucial stage is the thermal decomposition of core polymer SAN and the blend polymer PVP in shell. The electrodes were tested by using a practical two electrode symmetric system and displayed good electrochemical capacitive behaviors.

EXPERIMENTAL

Materials

Pyromellitic dianhydride (PMDA) ($M_w = 218.12$ g mol^{-1}), 4,4′-oxydianiline (ODA) ($M_w = 200.24$ g mol^{-1}), SAN ($M_w = 120{,}000$ g mol^{-1}), PVP ($M_w = 1300{,}000$ g mol^{-1}) (Sinopharm Chemical Reagent Co.), potassium hydroxide (KOH) (Beijing Modern Oriental Fine Chemistry Co.) and *N*, *N*-dimethylformamide (DMF) (Xilong Chemical Co.) were used as received.

Fabrication of Porous Hollow Carbon Nanofibers

The electrospinning shell-solution was prepared with 2.2 g PMDA, 2.0 g ODA, and 0.84 g PVP in 25 g DMF. The solution was stirred at 0°C for 24 h. The mass ratio of PVP was settled to be 20%. The electrospinning core-solution was prepared by dissolving SAN into DMF with 40 wt % and was kept at 80°C for 24 h.

A core–shell spinneret was used instead of a tube one. The flow rate of core and shell were controlled by two syringe pumps. The electrospinning setup illustration is shown in Figure 1(a). Parameters were set as follows: voltage of 20–25 kV, tip-to-collector distance of 25 cm, shell-solution flow of 0.8 mL h^{-1}, core-solution flow rate of 0 mL h^{-1}, 0.1 mL h^{-1}, 0.2 mL h^{-1}, 0.4 mL h^{-1}, and 0.6 mL h^{-1}. The obtained fibers were carbonized in a horizontal tubular furnace whose temperature was first increased to 300°C at 3°C min^{-1} and maintained for 30 min in compressed air atmosphere for the imidization of synthesized polyacrylic acid (PAA). Then the temperature was increased to 900°C at the same heating rate and maintained for 1 h under N_2 atmosphere for carbonization [Figure 1(b)]. N_2 worked as protective gas.

The carbon fibers with core-solution flow rate of 0 mL h^{-1}, 0.1 mL h^{-1}, 0.2 mL h^{-1}, 0.4 mL h^{-1}, and 0.6 mL h^{-1} were labeled as HCNF-0800, HCNF-0801, HCNF-0802, HCNF-0804, and HCNF-0806. The porous carbon fiber without hollow structure was labeled as PCNFs. The porous hollow carbon fiber was labeled as PHCNFs.

Characterization

The morphology of the nanofibers was investigated using LEO 1530 scanning electron microscope (SEM). X-ray diffraction (XRD) pattern of carbon fibers was examined with XRD (D/MAX-RM 2000) at the scanning rate of 5° min^{-1} in a range of diffraction angle 2θ from 10° to 60°. Raman spectra were recorded by HR800 (HORIBA spectrometer) with a wavelength of 633 nm to calculate the degree of crystallinity. The specific surface areas and pore-size distributions of the samples were evaluated by an automatic adsorption system (ASAP2020, Micromeritics) using the Brunauer–Emmett–Teller (BET) method. Pore size distribution was also derived from density functional theory (DFT) model.

A symmetrical two-electrode supercapacitor was assembled using two pieces of porous carbon nanofiber electrodes and a separator to investigate the electrochemical performance. To achieve sufficient electrolyte saturation in the electrodes and separator, they were previously immersed in 6*M* KOH solution under vacuum for 24 h before being assembled. Cyclic voltammetry (CV) and galvanostatic charge/discharge analysis were carried out to evaluate electrochemical performance of the electrodes with a potential window ranging from 0 to 1 V in 6*M* KOH electrolyte using an electrochemical workstation (CHI 600, Shanghai Chen Hua Instrument Company). The electrochemical impedance spectroscopy (EIS) was conducted in the frequency range of 0.01 Hz–100 kHz with perturbation amplitude of 5 mV versus the open circuit potential. The average specific capacitance was

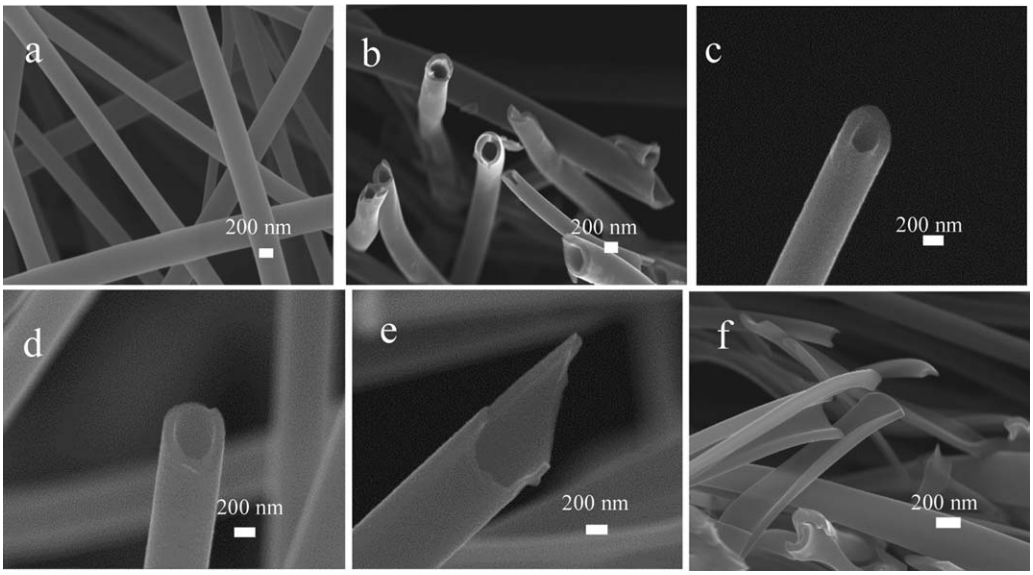

Figure 2. SEM images of (a) CNFs; (b) CNFs cross-section; (c) HCNF-0801; (d) HCNF-0802; (e) HCNF-0804; (f) HCNF-0806.

calculated according to the charge/discharge tests based on the following equation[18]:

$$C = 4\frac{I \cdot t}{m \cdot U}$$

where I, t, m, and U are the charge/discharge current (A), the discharge time (s), the total mass of active materials in the two electrodes (g), and the potential after the deduction of IR drop (V), respectively.

RESULTS AND DISCUSSION

The SEM images of porous hollow carbon fibers produced under different conditions are shown in Figure 2. The fiber diameters are all around 400–500 nm as shown in Figure 2(a). The cross-section of the fibers shown in Figure 2(b) clearly demonstrates that uniformly hollowed structure was successfully achieved. It should be mentioned that only the fibers obtained with internal flow rate two times lower than the external flow rate showed morphology free of defects. With the increase of the flow rate of SAN in the inner core, it is found that the inner diameter of PHCNFs increases and the wall thickness decreases. When the inner flow rate reaches 0.6 mL h^{-1}, the shell of the fiber collapses as shown in Figure 2(f).

XRD was employed to monitor the structure of hollow carbon fibers. As shown in Figure 3(a), the diffraction peaks at $2\theta = 24°$ and 44°can be attributed to the development of (002) and 10 planes, respectively, which confirms that the fibers are in turbostratic microstructure.[19] The crystallinity was confirmed by the following Raman spectra in Figure 3(b). The two bands at about 1330 and 1590 cm^{-1} are ascribed to the D- and G-band of carbon materials[20] as shown in Figure 3(b). The intensity ratio I_D/I_G was calculated to be about 1.9, indicating a turbostratic structure of the CNFs.

N_2 adsorption/desorption measurement was performed to characterize the specific surface area and the pore-size distribution of the samples. The resulting isotherms and pore-size distributions calculated by DFT method are displayed in Figure 4. All isotherms are typical IUPAC type I [Figure 4(a)], suggesting the dominant microporous structure. Horizontal isotherms without

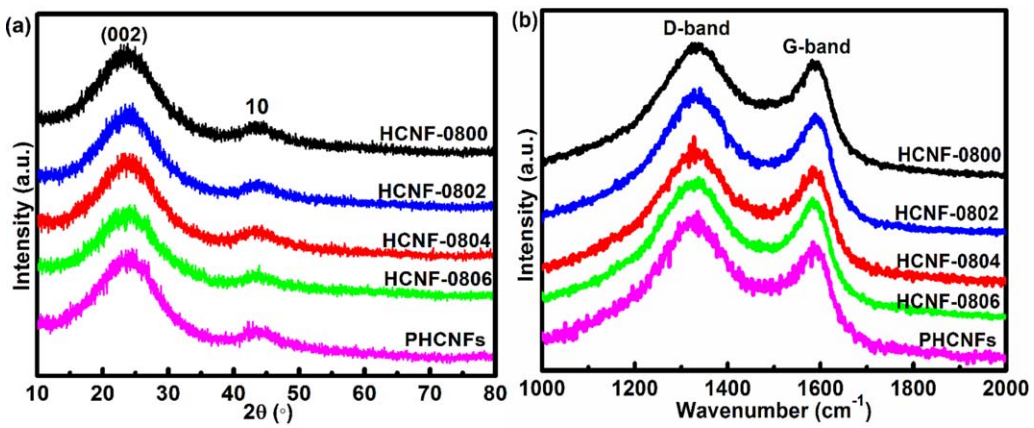

Figure 3. (a) XRD results of HCNFs and PHCNFs; (b) Raman spectra of HCNFs and PHCNFs. [Color figure can be viewed in the online issue, which is available at wileyonlinelibrary.com.]

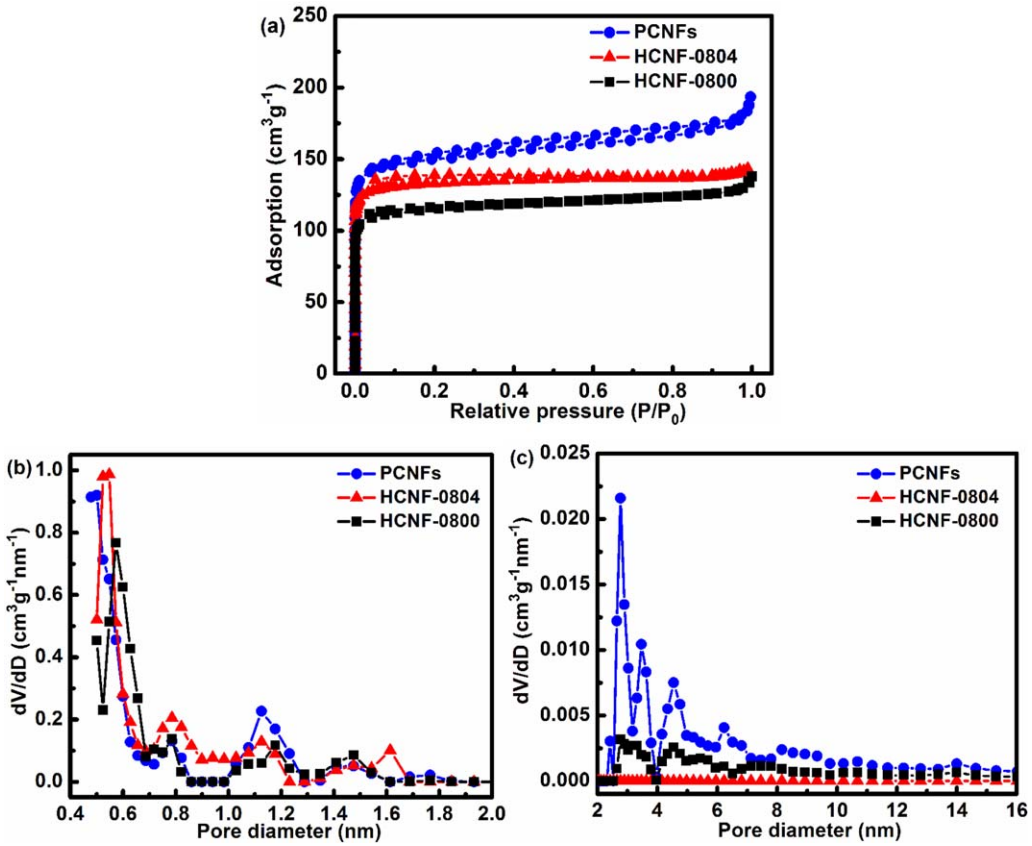

Figure 4. (a) N_2 adsorption/desorption isotherms of PCNFs, HCNF-0804, and HCNF-0800; (b, c) DFT pore size distributions of PCNFs, HCNF-0804, and HCNF-0800. [Color figure can be viewed in the online issue, which is available at wileyonlinelibrary.com.]

hysteresis loops are shown with HCNF-0800 and HCNF-0804, which reflect the microporous structures. With PCNFs, an obvious hysteresis loop appears in isotherm curve, revealing the existence of mesoporous structure.[21] In addition, PCNFs owns the largest specific surface areas and pore volumes among the samples. In Figure 4(b, c), the pore-size distributions of these samples are compared by dividing into two regions, micropore and mesopore regions, respectively. As can be seen in Figure 4(b), HCNF-0804 and PCNFs share an evident increase of pores at 0.5 nm, 0.8 nm, and 1.2 nm. In Figure 4(c), PCNFs shows abundant peaks in a range of 2–8 nm, but no marked peak is recognized on other samples. These mesopores are especially beneficial for ion transfer and could thus optimize the performance of materials under large current. Specific surface area and specific total volume of materials are displayed in Table I. HCNF-0800, HCNF-0804, and PCNFs possess a specific surface area of 456 $m^2\ g^{-1}$, 539 $m^2\ g^{-1}$, and 603 $m^2\ g^{-1}$, respectively. Pores whose diameters are over 0.7 nm in HCNF-0804 make great contribution to the increment of specific surface area of the material, so do pores whose diameters are smaller than 0.7 nm in PCNFs. Since SAN is a tube inducer, we can attribute the appearance of new pores in HCNF-0804 to the thermal decomposition of core polymer SAN. New pores in 2–8 nm in PCNFs are mainly contributed by PVP additive.

To optimize the inner diameter of the carbon fiber electrode, first of all, CV test was performed at 100 mV s^{-1} with HCNFs [Figure 5(a)]. It could be seen that a quasi-rectangular shape were received with hollow fibers with different inner diameters; while a twisted rectangular shape was received with solid fibers.

Table I. Specific Surface Area and Specific Total Volume of Materials

Fibers	S_{BET} ($m^2\ g^{-1}$)	$S_{<0.7\ nm}$ ($m^2\ g^{-1}$)	$S_{0.7\text{-}2\ nm}$ ($m^2\ g^{-1}$)	$S_{>2\ nm}$ ($m^2\ g^{-1}$)	V_{total} ($cm^3\ g^{-1}$)	$V_{<0.7\ nm}$ ($cm^3\ g^{-1}$)	$V_{0.7\text{-}2\ nm}$ ($cm^3\ g^{-1}$)	$V_{>2\ nm}$ ($cm^3\ g^{-1}$)
HCNF-0800	456	388	64	4	0.201	0.140	0.043	0.018
HCNF-0804	539	423	116	0	0.221	0.144	0.077	0
PCNFs	603	512	79	12	0.291	0.181	0062	0048

$S_{<0.7\ nm}$: specific surface area with pore diameter of 0–0.7 nm.
$S_{0.7\text{-}2\ nm}$: specific surface area with pore diameter of 0.7–2 nm.
$S_{>2\ nm}$: specific surface area with pore diameter above 2 nm.

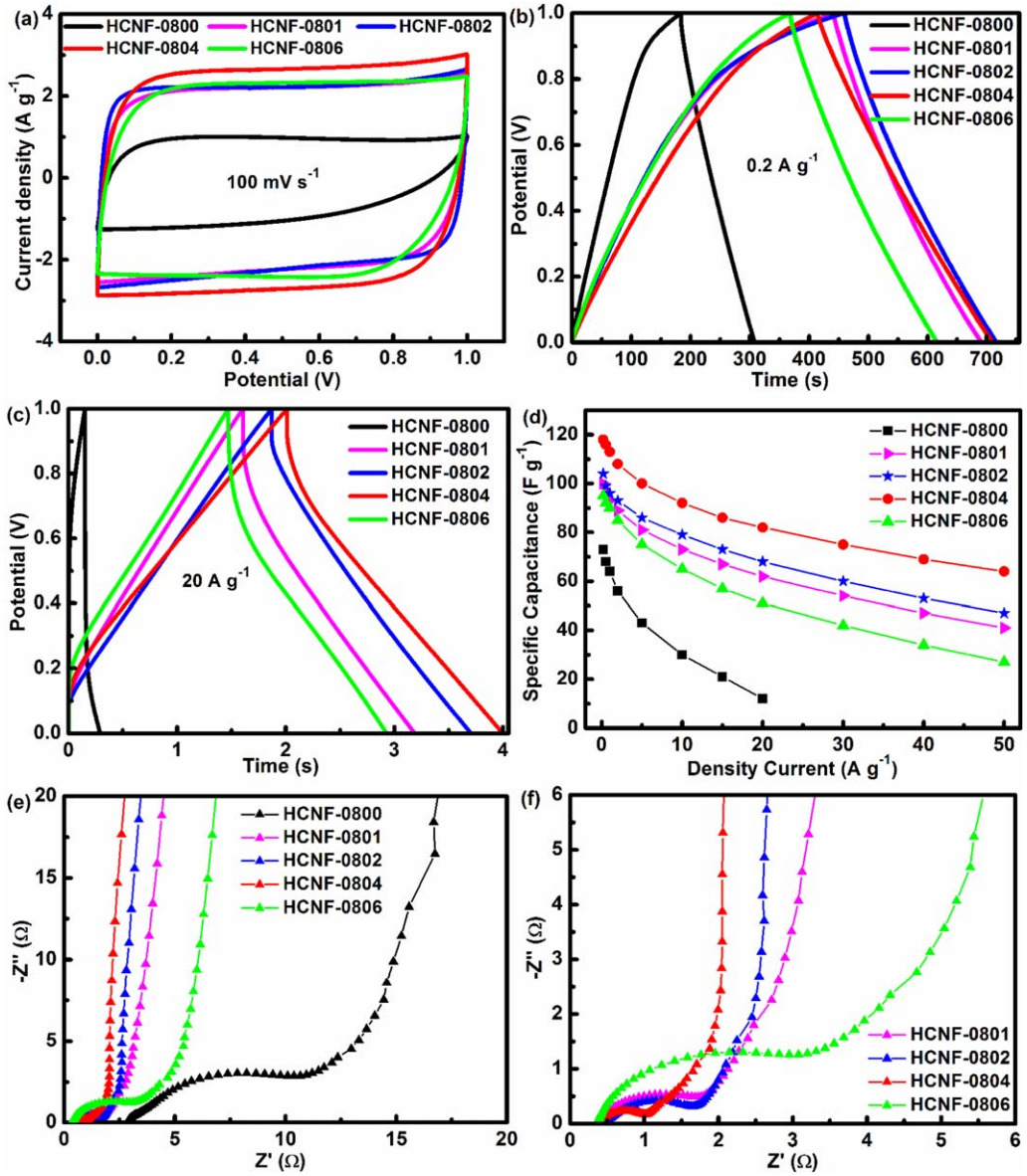

Figure 5. (a) CV curves; (b) galvanostatic charging/discharging at 0.2 A g^{-1}; (c) at 20 A g^{-1}; (d) SC values of HCNFs; (e, f) EIS Nyquist spectra. [Color figure can be viewed in the online issue, which is available at wileyonlinelibrary.com.]

Among HCNFs, the curve of HCNF-0804 encloses the largest area, indicating that HCNF-0804 owns the biggest specific capacitance in our test.

As depicted in Figure 5(b, c), galvanostatic charging/discharging test of HCNF-0800 and HCNFs were performed under current densities of 0.2 A g^{-1} and 20 A g^{-1}, respectively. All curves present a quasi-symmetric triangular shape in Figure 5(b) at a high current density of 20 A g^{-1}, suggesting a double layer capacitance performance from ion adsorption and desorption process. At lower charge and discharge current density, 2 A g^{-1}, the curve of HCNF-0800 loses its symmetry. The specific capacitance of HCNF-0800, HCNF-0801, HCNF-0802, HCNF-0804, and HCNF-0806 are 73 F g^{-1}, 100 F g^{-1}, 104 F g^{-1}, 118 F g^{-1}, and 95 F g^{-1} calculated based on the data at the current density of 0.2 A g^{-1}. It can clearly be seen, the specific capacitance keeps increasing with the decline of wall thickness before the tube collapses.

Nyquist plots of the cells are shown in Figure 5(e,f). The semicircle at high frequency zone represents the charge-transfer resistance accompanied with migration of ions between the electrode and electrolyte interface, and the straight slopping line corresponds to the diffusion of ion in the active material of electrode. It is interesting to find that HCNF-0804 shows the largest ionic conductivity and the lowest interfacial resistance of 0.6 ohm.

To improve the specific capacitance of the electrode, PVP was introduced into the shell solution of HCNF-0804 as pore inducer in the carbonization process.

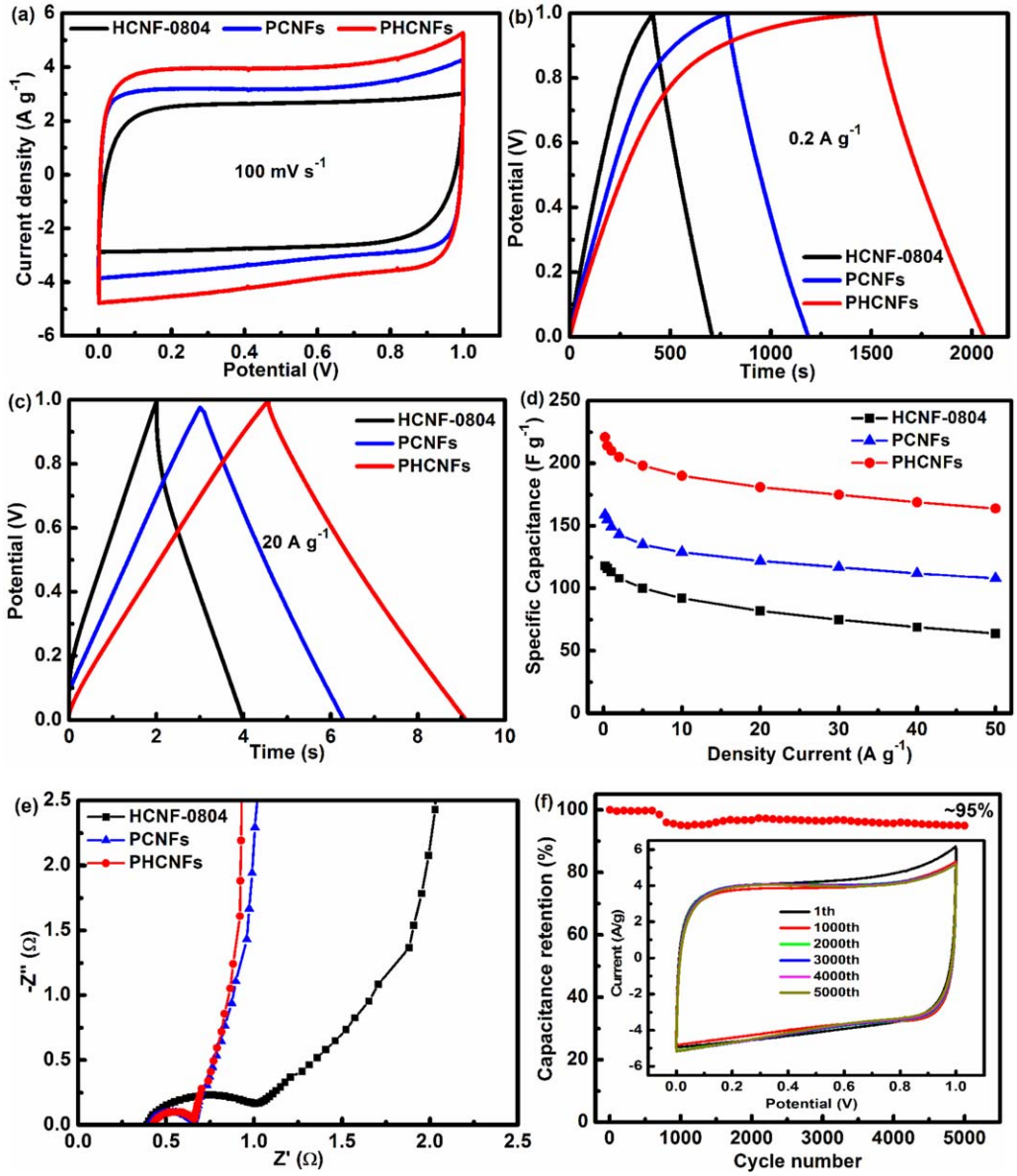

Figure 6. (a) CV curves; (b) galvanostatic charging/discharging at 0.2 A g^{-1}; (c) at 20 A g^{-1}; (d) SC values of HCNF-0804, PCNFs, and PHCNFs; (e) EIS Nyquist spectra; (f) variations of normalized capacitance retention of PHCNFs. [Color figure can be viewed in the online issue, which is available at wileyonlinelibrary.com.]

CV test was performed as shown in Figure 6(a). To get more insights into the advantages of the PHCNFs electrode, HCNFs, PCNFs were developed and tested for comparison. It could be seen that a quasi-rectangular shape was received with all of the three samples. The curve of PHCNFs encloses the largest area, indicating that PHCNFs own the biggest specific capacitance.

Galvanostatic charging/discharging test of HCNF-0804, PCNFs, and PHCNFs were performed at both current densities of 0.2 A g^{-1} and 20 A g^{-1}, and the results are displayed in Figure 6(b,c).

As can be observed, the curves present a quasi-symmetric triangular shape in Figure 6(c) at a current density of 20 A g^{-1}, suggesting a double layer capacitance performance from ion adsorption and desorption process. At lower charge and discharge current density, 0.2 A g^{-1}, the curve of HCNF-0800 loses its symmetry, revealing the nature of pseudocapacitor, which can be attributed to the introduction of nitrogen of PVP.[10] At the current density of 0.2 A g^{-1}, the specific capacitance of HCNF-0804, PCNFs, and PHCNFs are 118 F g^{-1}, 159 F g^{-1}, 221 F g^{-1}, respectively [Figure 6(d)]. The value is well in the hollow carbon nanofibers electrode of supercapaciors.[11,22]

Moreover, as can be seen in EIS Nyquist spectra [Figure 6(e)], PHCNFs show a much smaller charge transfer resistance (0.23 ohm), than that of HCNFs (0.6 ohm).

The capacitance retention test of PHCNFs was performed at a scan rate of 100 mV s^{-1} [Figure 6(f)]. After 5000 cycles, PHCNFs electrodes can keep 95% of its capacitance.

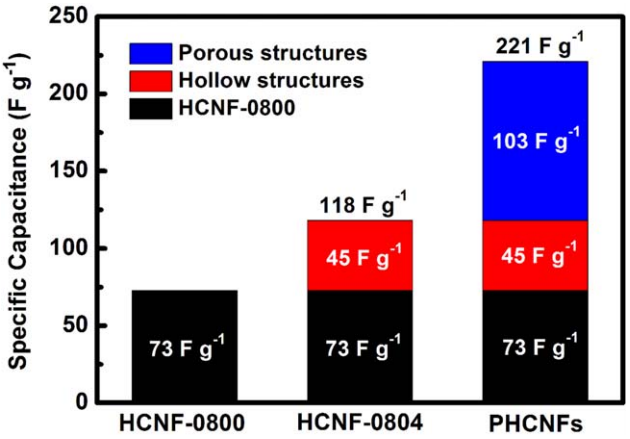

Figure 7. Contribution of hollow and porous structures to the specific capacitance. [Color figure can be viewed in the online issue, which is available at wileyonlinelibrary.com.]

The high capacitance of PHCNFs electrode could be contributed by the hollow structure and the porous structure of the fiber. The hollow structure in HCNFs and PHCNFs can be regarded as a channel to improve the ions transportation in the bulk of the electrode. Ions are able to transport to both the outer and inner surfaces of the tube, which increases the specific surface capacitance of electrodes. The specific capacitance can be improved by micropores derived from PVP on the thin tube wall for charge storage. The contribution of hollow and porous structures to the specific capacitance is displayed in Figure 7. It can be inferred that hollow structures bring a 20% capacitance improvement, while the porous morphology brings a 47% capacitance improvement.

CONCLUSIONS

Porous hollow carbon nanofibers using SAN solution as core and PAA as shell were manufactured by co-axial electrospinning technique, taking PVP as a pore inducer additive in the shell. The hollow structure in PHCNFs can be regarded as a channel to improve the ions transportation in the bulk of the electrode. Ions are able to transport to both the outer and inner surfaces of the tube, which increases the specific surface capacitance of electrodes. The specific capacitance can be improved by micropores derived from PVP on the thin tube wall for charge storage. By controlling the shell wall thickness of PHCNFs, we found that the optimized PHCNF-0804 could provide a high specific capacitance of 221 F g^{-1} and remaining a capacitance retention of 95% after 5000 cycles under a scan rate of 0.1 V s^{-1}. In this system, hollow structures bring a 20% capacitance improvement, while the porous morphology brings a 47% capacitance improvement. The attractive performances exhibited by these sponge supercapacitors make them potentially promising candidates for future energy storage systems.

ACKNOWLEDGMENTS

The authors acknowledge the fund from the National Natural Science Foundation of China (No. 51572174). Supported by State Key Laboratory of Electrical Insulation and Power Equipment (EIPE14212)

REFERENCES

1. Portet, C.; Taberna, P. L.; Simon, P.; Flahaut, E.; Laberty-Robert, C. *Electrochim. Acta* **2005**, *50*, 4174.
2. Gamby, J.; Taberna, P. L.; Simon, P.; Fauvarque, J. F.; Chesneau, M. *J. Power Sources* **2001**, *101*, 109.
3. Sun, G.; Wang, J.; Liu, X.; Long, D.; Qiao, W.; Ling, L. *J. Phys. Chem. C* **2010**, *114*, 18745.
4. Huang, X.; Kim, S.; Heo, M. S.; Kim, J. E.; Suh, H.; Kim, I. *Langmuir* **2013**, *29*, 12266.
5. Xu, F.; Cai, R. J.; Zeng, Q. C.; Zou, C.; Wu, D. C.; Li, F.; Lu, X.; Liang, Y. R.; Fu, R. W. *J. Mater. Chem.* **2011**, *21*, 1970.
6. Lai, X. Y.; Halpert, J. E.; Wang, D. *Energ. Environ. Sci.* **2012**, *5*, 5604.
7. Han, Y.; Dong, X.; Zhang, C.; Liu, S. *J. Power Sources* **2012**, *211*, 92.
8. Hulicova, D.; Oya, A. *Carbon* **2003**, *41*, 1443.
9. Inagaki, M.; Yang, Y.; Kang, F. *Adv. Mater.* **2012**, *24*, 2547.
10. Le, T. H.; Yang, Y.; Huang, Z. H.; Kang, F. *J. Power Sources* **2015**, *278*, 683.
11. Xu, Q.; Yu, X. L.; Liang, Q. H.; Bai, Y.; Huang, Z. H.; Kang, F. *J. Electroanal. Chem.* **2015**, *739*, 84.
12. Sun, D.; Qin, G.; Miao, L.; Wei, W.; Wang, N.; Jiang, L. *Carbon* **2013**, *63*, 585.
13. Kim, B. H.; Yang, K. S.; Ferraris, J. P. *Electrochim. Acta* **2012**, *75*, 325.
14. Nicole, E. Z.; Kenneth, E. S.; Joshua, A. O.; Adam, M. R.; Thomas, P. B. *J. Phys. Chem. B* **2011**, *115*, 12441.
15. Lee, B. S.; Son, S. B.; Park, K. M.; Lee, G.; Oh, K. H.; Lee, S. H. *ACS Appl. Mater. Interfaces* **2012**, *4*, 6701.
16. Lallave, M.; Bedia, J.; Ruiz-Rosas, R.; Rodríguez-Mirasol, J.; Cordero, T.; Otero, J. *Adv. Mater.* **2007**, *19*, 4292.
17. Lee, B. S.; Park, K. M.; Yu, W. R.; Ji, H. Y. *Macromol. Res.* **2012**, *20*, 605.
18. Tan, Y. M.; Xu, C. F.; Chen, G. X.; Liu, Z. H.; Ma, M.; Xie, Q. J.; Zheng, N. F.; Yao, S. Z. *ACS Appl. Mater. Interfaces* **2013**, *5*, 2241.
19. Zhai, Y.; Wan, Y.; Cheng, Y. *J. Porous Mater.* **2008**, *15*, 601.
20. Ferrari, A. C.; Robertson, J. *Phys. Rev. B* **2000**, *61*, 14095.
21. Lowell, S.; Shield, J. E.; Thomas, M. A.; Thommes, M. Characterization of Porous Solids and Powders: Surface Area, Pore Size, and Density; Springer: The Netherlands, **2006**; Vol. *16*, Chapter 5, p 43.
22. El-Deen, A. G.; Barakat, N. A. M.; Khalil, K. A.; Kim, H. Y. *New J. Chem.* **2013**, *38*, 198.